Inorganic Chemistry

Article

pubs.acs.org/IC

Silver Indium Telluride Semiconductors and Their Solid Solutions with Cadmium Indium Telluride: Structure and Physical Properties

Simon Welzmiller,[†] Felix Hennersdorf,[†] Robert Schlegel,[†] Andrew Fitch,[‡] Gerald Wagner,[†] and Oliver Oeckler*,[†]

[†]Faculty of Chemistry and Mineralogy, Leipzig University, Scharnhorststraße 20, 04275 Leipzig, Germany

[‡]ESRF—The European Synchrotron; 71, Avenue des Martyrs, 38043 Grenoble Cedex 9, France

Supporting Information

ABSTRACT: $Ag_{0.8}In_{2.4}Te_4$ (= $AgIn_3Te_5$) and $Ag_{0.5}In_{2.5}Te_4$ (= $AgIn_5Te_8$) form solid solutions with $CdIn_2Te_4$, which are interesting as materials for photovoltaics or with respect to their thermoelectric properties. The corresponding crystal structures are related to the chalcopyrite type. Rietveld refinements of high-resolution synchrotron powder diffraction data measured at K-absorption edges of Cd, Ag, In, and Te and electron diffraction reveal the symmetry as well as the element and vacancy distribution in $Ag_{0.8}In_{2.4}Te_4$ (= $AgIn_3Te_5$)/$Ag_{0.5}In_{2.5}Te_4$ (= $AgIn_5Te_8$) mixed crystals such as $Ag_{0.25}Cd_{0.5}In_{2.25}Te_4$ and $Ag_{0.2}Cd_{0.75}In_{2.1}Te_4$. All compounds of the solid solution series $(CdIn_2Te_4)_x(Ag_{0.5}In_{2.5}Te_4)_{1-x}$ exhibit the $HgCu_2I_4$ structure type (space group $I\bar{4}2m$) with completely ordered vacancies but disordered cations. The uniform cation distribution and thus the local charge balance are comparable to that of $CdIn_2Te_4$. In contrast, $Ag_{0.8}In_{2.4}Te_4$ (= $AgIn_3Te_5$) crystallizes in the space group $P\bar{4}2c$ with disordered cations and partially ordered vacancies. This is corroborated by bond-valence sum calculations and the fact that there is a Vegard-like behavior for compounds with $0.5 < x$ in the pseudobinary system $(CdIn_2Te_4)_x(Ag_{0.8}In_{2.4}Te_4)_{1-x}$. Owing to the different structures, there is no complete solid solution series between $CdIn_2Te_4$ and $AgIn_3Te_5$. All compounds in this work are n-type semiconductors with a low electrical conductivity (~1 S/m) and rather high absolute Seebeck coefficients (up to −750 μV/mK; 225 °C). Electrical band gaps (E_g) determined from the Seebeck coefficients as well as (more reliably) from the electrical conductivity range between 0.19 and 1.13 eV.

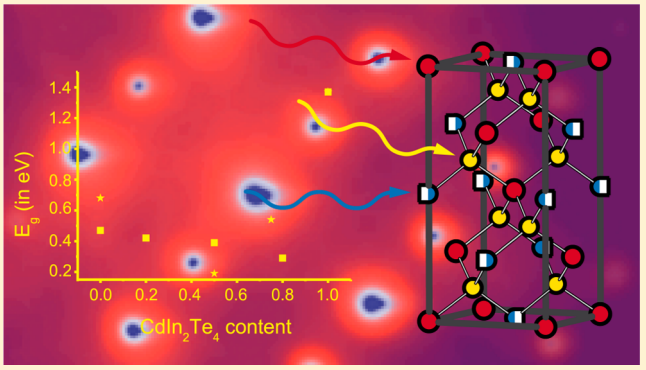

INTRODUCTION

Among the plethora of compounds with tetrahedral coordination of all atoms, those derived from the sphalerite (ZnS) structure type (space group $F\bar{4}3m$) are most notable. Many of them are multinary chalcogenides, which attracted much attention as promising materials for solar cells or thermoelectric power generation. CdTe, for example, reaches cell efficiencies of up to 16.7% in photovoltaic applications.[1] $Cu(In,Ga)(Se,S)_2$ compounds with efficiencies of up to 20.4% exhibit chalcopyrite-type structures ($FeCuS_2$, space group $I\bar{4}2d$), which is an ordered variant of the sphalerite type.[2−4] The related kesterites also form an ordered variant of the sphalerite type and reach cell efficiencies of up to 9.7%, but contain more abundant and less toxic elements such as Zn or Sn.[5] Concerning thermoelectric properties, $Cu_2CdSnSe_4$ and $Ag_{1-x}GaTe_2$ (x = 0.03) have figures of merit (ZT) of up to 0.7 at ~400 °C and 0.8 at ~580 °C, respectively.[3,6] First-principles calculations indicate the possibility of even higher ZT values upon p-doping for $AgGaTe_2$ and related materials such as $CdGeAs_2$ or $CdSnAs_2$.[7,8]

Among the stable compounds known in the system Ag_2Te−In_2Te_3, $AgInTe_2$ and a Ag-poor phase $Ag_3In_{97}Te_{147}$ are stoichiometric, while both $AgIn_5Te_8$ (= $Ag_{0.5}In_{2.5}Te_4$) and $AgIn_3Te_5$ (= $Ag_{0.8}In_{2.4}Te_4$) exhibit a broad homogeneity range.[9−12] Ag_2Te, which is known as the mineral hessite, forms a network built up from distorted tetrahedra interconnected via both vertices and edges (space group $P2_1/c$).[13] It undergoes a phase transition at ~150 °C, where a cubic high-temperature (HT) phase (space group $Fm\bar{3}m$) with dynamical Ag ion disorder is formed.[14] In contrast, the room-temperature (RT) phase of In_2Te_3 forms a superstructure of the sphalerite type (space group $F\bar{4}3m$) with ordered cation vacancies[15] as well as a sphalerite-type HT phase with disordered vacancies.[16] $AgIn_5Te_8$ (= $Ag_{0.5}In_{2.5}Te_4$) was first described with ordered vacancies in space group $I\bar{4}$ ($CdGa_2S_4$ structure type), with two Wyckoff sites 2*a* and 2*c* occupied by In and one site 2*b* shared by equal amounts of Ag and In.[17,18] A later investigation[19] favors the $AgIn_5Se_8$ structure type,[20] which exhibits completely ordered cations (Wyckoff sites 1*a* and 4*m* In; 1*b* Ag) and vacancies in space group $P\bar{4}2m$. Thermoelectric measurements of $AgIn_5Te_8$ yield a ZT value of ~0.005 at 580

Received: February 22, 2015
Published: May 29, 2015

DOI: 10.1021/acs.inorgchem.5b00433
Inorg. Chem. 2015, 54, 5745−5756

°C, again limited by the low electrical conductivity of ∼1 S/cm combined with a Seebeck coefficient of ∼170 μV/K; the optical band gap is ∼1 eV.[21] Concerning the structure of $AgIn_3Te_5$, models related to $CuIn_3(Te/Se)_5$ assuming the "thiogallate" (space group $I\bar{4}$)[22] and stannite (Cu_2FeSnS_4, space group $I\bar{4}2m$)[23] structure types as well as another tetragonal model (space group $P\bar{4}2c$)[24−26] have been discussed. Based on Rietveld refinements with laboratory X-ray data as well as electron diffraction, a recent study[27] concludes that $AgIn_3Te_5$ most likely exhibits $P\bar{4}2c$ symmetry with partially disordered vacancies. Yet, the atom distribution is still not unequivocally determined due to lacking scattering contrast.

$AgIn_3Te_5$, better written as $Ag_{0.8}In_{2.4}Te_4$ according to the cell content, exhibits a very low ZT value of 0.000 18 at ∼180 °C, owing to its very low electrical conductivity (0.01 S/cm), which is consistent with an electrical band gap of ∼1.13 eV.[12] Chalcopyrite-type $AgInTe_2$[28] and $Ag_{1-x}InTe_2$, a Ag-deficient variant, also show low ZT values of ∼0.007 at ∼300 °C due to their low electrical conductivities of ∼0.2 S/cm.[29] Thin films of $AgInTe_2$ exhibit an anomalous photovoltaic effect due to their anisotropic growth.[30] In chalcopyrite-type solid solutions between $AgInTe_2$ and $CdIn_2Te_4$, i.e., $(CdIn_2Te_4)_x(Ag_2In_2Te_4)_{1-x}$ with $x < 0.5$, the optical band gap increases from ∼0.95 eV to ∼1.13 eV with increasing $CdIn_2Te_4$ content and thus increasing vacancy concentration.[31] $CdIn_2Te_4$ itself is a semiconductor with an electrical band gap of ∼1.4 eV[32] and forms a defect chalcopyrite-type structure with 25% cation vacancies. It was first described in space group $I\bar{4}$,[33] but a later analysis using synchrotron radiation revealed that it crystallizes in space group $I\bar{4}2m$,[34] which was confirmed by an anomalous dispersion study, which also revealed the disordered element distribution.[35]

Multinary chalcopyrite-type and related semiconductors often contain elements with similar electron counts (e.g., Cd, Ag, In, Sn, Te), which cannot be effectively distinguished either by conventional X-ray scattering or by neutron scattering due to low scattering contrast. This problem can be overcome by resonant X-ray scattering, when the (energy- but not angle-dependent) anomalous dispersion terms of the atomic form factor f, i.e., the real part $\Delta f'$ and the imaginary part $\Delta f''$, increase at the absorption edges of elements. $\Delta f'$ then becomes significantly negative, so that the corresponding element appears to have fewer electrons. Reliable values for $\Delta f'$ are as crucial as joint refinements on data sets at different wavelengths (near absorption edges and also away from them) in order to refine the element distribution.[36] This technique was recently applied to determine the element distribution in single crystals of layered compounds in the system Ge/Sn/Sb/Te[37,38] as well as for $Ge_2Sb_2Te_5$,[39] $Ge_3SbInTe_6$,[40] and $SnSb_2Te_4$.[41] Compounds with tetrahedral coordination like kesterites[42] as well as $Ba_8Ga_{16}Ge_{30}$[43] or GaAs/AlAs multilayer systems[44] were also analyzed in the same fashion. Despite the lower precision, anomalous dispersion was also exploited in powder diffraction studies, e.g., for clathrates,[45] sulfosalt-like materials,[46] or chalcopyrite-like materials such as $CdIn_2Te_4$ and compounds from the solid solution $(CdIn_2Te_4)_x(Ag_2In_2Te_4)_{1-x}$.[35] The latter investigation revealed that vacancies tend to order but that cation sites exhibit mixed occupancies.

In the present study, we address the open question of element and vacancy ordering in $AgIn_3Te_5$ (= $Ag_{0.8}In_{2.4}Te_4$) and $AgIn_5Te_8$ (= $Ag_{0.5}In_{2.5}Te_4$), respectively, and their solid solutions with $CdIn_2Te_4$ as far as they exist, and the effect of the composition on electrical properties. Resonant X-ray diffraction at the K absorption edges of all elements involved is an ideal tool to elucidate the symmetry and element distribution for various $CdIn_2Te_4$ contents associated with different vacancy concentrations. In contrast to single crystals grown from the gas phase, powdered homogeneous samples ensure an exactly defined chemical composition.

EXPERIMENTAL SECTION

Sample Preparation. All samples were prepared by melting stochiometric amounts of the elements or ternary compounds in sealed silica ampules under a dry Ar atmosphere, in some cases followed by annealing. The respective ternary compounds $Ag_{0.8}In_{2.4}Te_4$, $Ag_{0.5}In_{2.5}Te_4$, and $CdIn_2Te_4$ were synthesized from pure elements Ag (99.999%, Premion), Cd (99.9999%, Koch Chemicals), In (99.999%, VEB Spurenmetalle Freiberg), and Te (puriss., VEB Spurenmetalle Freiberg) by quenching corresponding melts in water. Quaternary compounds were prepared by melting stoichiometric amounts of ternary compounds at 950 or 690 °C followed by annealing at 690 or 450 °C (for detailed information see Table S1 in the Supporting Information). For the measurement of Seebeck coefficients and electrical conductivities, disc-shaped samples (20 mm diameter; 2.5 g) were prepared by melting stochiometric amounts of elements (700 °C for 12 h and 920 °C for 24 h) in silica ampules with a flat bottom, quenching in air, and subsequent annealing at 600 °C for 72 h followed by quenching in air. The ingots obtained were ground to obtain plane-parallel discs. Cuboid samples were cut out of the discs using a diamond wire saw and subsequently polished using a lapping disc.

Electron Microscopy and X-ray Spectroscopy. The homogeneity and composition were investigated by means of energy-dispersive X-ray spectroscopy (EDX) using a LEO 1530 Gemini (Zeiss) scanning electron microscope (SEM) equipped with an EDX detector (INCA software, Oxford Instruments). Representative parts of the sample were crushed and fixed on conducting carbon tabs. Approximately horizontal faces were used for EDX measurements.

Transmission electron microscopy (TEM) was done with a Philips STEM CM-200 ST (acceleration voltage 200 kV, point resolution 0.23 nm) equipped with an EDX system (EDAX). Parts of the samples were embedded in epoxide resin, cut, and thinned by dimple grinding, followed by Ar ion thinning (Gatan Duo-Mill). The kinematical approximation was used for the calculation of electron diffraction patterns (SAED, selected area electron diffraction) with the JEMS[47] program package.

X-ray Powder Diffraction. Laboratory X-ray powder patterns for the investigation of sample homogeneity and lattice parameter determination were recorded using a Huber G670 Guinier camera with fixed imaging-plate detector and automatic read-out system (Cu-$K_{\alpha 1}$ radiation, Ge(111) monochromator, λ = 1.540 56 Å). Representative parts of the samples were powdered and fixed on a specimen holder with Mylar foil using hair-fixing spray.

Synchrotron powder diffraction data of samples in glass capillaries (borate glass, 0.3 mm diameter, spun in order to enhance particle distribution statistics) were acquired at Beamline ID 31 (ESRF, Grenoble, France) using a Debye−Scherrer setup and an array of nine point detectors with Si(111) analyzer crystals.[48] Data were measured in continuous scan mode and afterward merged, taking into account the offset calibrated using a NIST Si 670c standard sample.[49] The latter was also used to precisely determine the wavelength of 0.354198(10) Å (35.004 keV) necessary for measurements far from absorption edges. Energies near the K-absorption edges of Ag, Cd, In, and Te were chosen slightly at the low-energy side of the edges (for exact values, cf. Tables 1, 3, 5, and 7), which were determined individually for each compound by fluorescence measurements (AXAS 10MM2, KETEK GmbH). Anomalous dispersion correction terms were calculated from the characteristic X-ray fluorescence of the respective element as a function of the wavelength of the incident radiation, employing the Kramers−Kronig transform[50] provided by the program CHOOCH.[51] Other dispersion correction terms were taken from ref 52.

DOI: 10.1021/acs.inorgchem.5b00433
Inorg. Chem. 2015, 54, 5745−5756

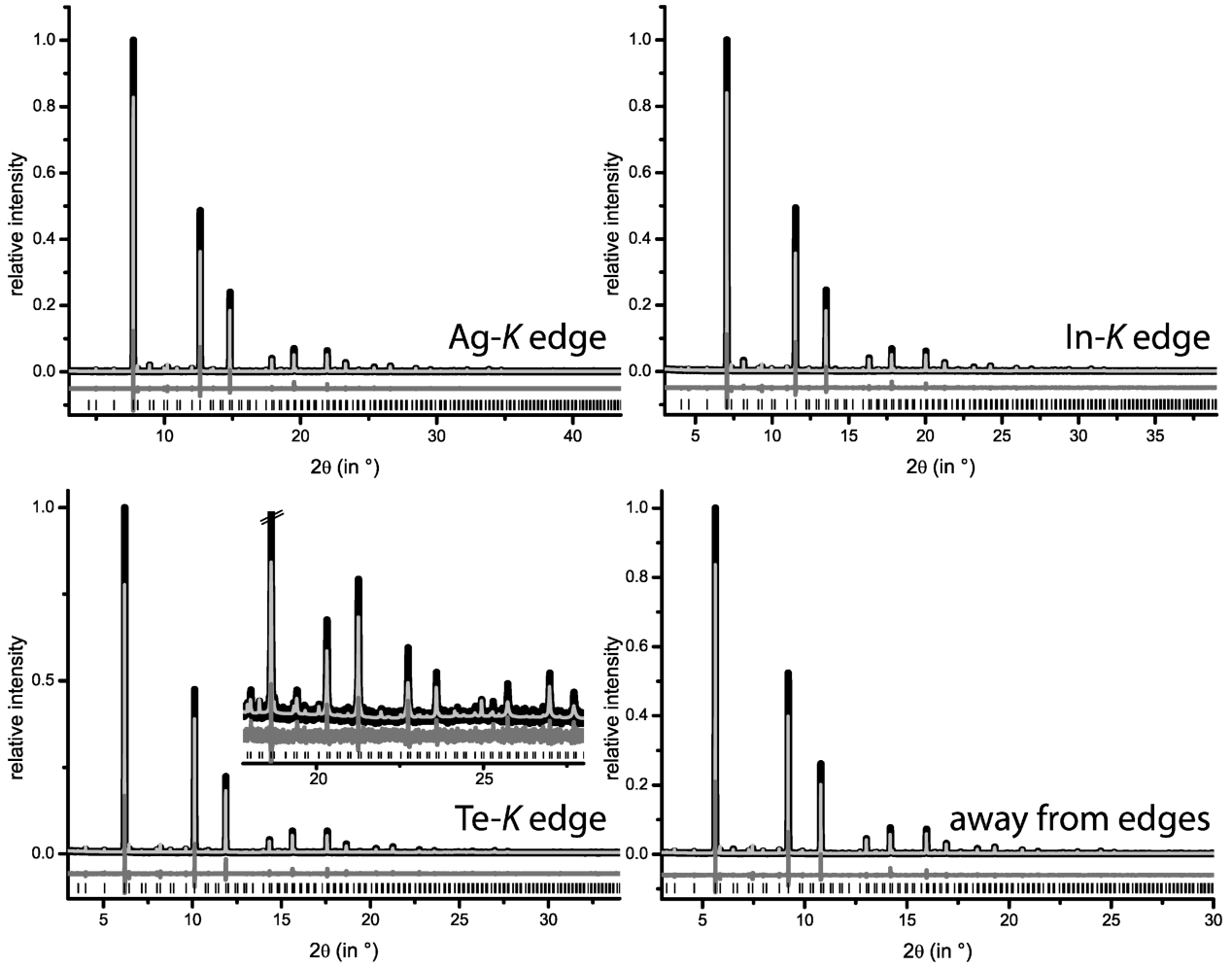

Figure 1. Results of the joint Rietveld refinement for $AgIn_3Te_5$ = $Ag_{0.8}In_{2.4}Te_4$ for wavelengths at the Ag-K, In-K, and Te-K edges as well as away from them (cf. Table 1): vertical lines indicate calculated reflection positions; experimental (black) and calculated intensities (gray) as well as difference plots (below; same intensity scale as the diffraction patterns) are shown (inset: enlargement of the high-angle region); enlarged patterns are depicted in the Supporting Information (Figures S1−S4).

Rietveld Refinements. Rietveld and Pawley fits were performed with Topas Academic;[53] reflection profiles were described using a direct convolution approach with fundamental parameters and an emission profile described by the combination of a Lorentzian and a Gaussian function. Data measured at the K-edges of elements involved and away from the edges were employed in order to elucidate the element distribution in $AgIn_3Te_5$, $Ag_{0.2}Cd_{0.75}In_{2.1}Te_4$, $AgIn_5Te_8$, and $Ag_{0.25}Cd_{0.5}In_{2.25}Te_4$ by joint refinements on all data sets. The off-edge wavelength was fixed as determined from the Si standard sample. It was used for the determination of precise lattice parameters and as a reference for the refinement of the other wavelengths, which turned out not to deviate more than 0.01% (typically a 3σ range) from the ones calculated from the monochromator angle. The background of each diffraction pattern was fitted by a set of 24 individual parameters (shifted Chebychev function). Preferred orientation was taken into account by spherical harmonics of the fourth grade with an individual set of parameters for each diffraction pattern, which proved necessary, as the degree of preferred orientation slightly depends on the region of the capillary irradiated. Microstrain was considered by the convolution of a Lorentzian and a Gaussian function for the refinements of $AgIn_5Te_8$ and $Ag_{0.25}Cd_{0.5}In_{2.25}Te_4$; in the other refinements a numerical model for anisotropic peak broadening was used.[54] Refinements on laboratory data sets were carried out only for lattice parameter determination. All diffraction patterns with the corresponding Rietveld fits ($AgIn_3Te_5$: Figures S1−S4; $Ag_{0.2}Cd_{0.75}In_{2.1}Te_4$: Figures S5−S9; $AgIn_5Te_8$: Figures S10−S13; $Ag_{0.25}Cd_{0.5}In_{2.25}Te_4$: Figures S14−S18; $Ag_{0.4}Cd_{0.5}In_{2.2}Te_4$: Figure S19; $Ag_{0.4}Cd_{0.2}In_{2.4}Te_4$: Figure S20; $Ag_{0.3}Cd_{0.4}In_{2.3}Te_4$: Figure S21; $Ag_{0.2}Cd_{0.6}In_{2.2}Te_4$: Figure S22; $Ag_{0.1}Cd_{0.8}In_{2.1}Te_4$: Figure S23) as well as the results of refinements under laboratory conditions (cf. Tables S2−S5) are shown in the Supporting Information. Selected diffraction patterns are shown in Figures 1, 3, 7, and 10. Further details of the crystal structure determinations are available from the Fachinformationszentrum Karlsruhe, D-76344 Eggenstein-Leopoldshafen (Germany), on quoting the depository numbers CSD-429086 ($AgIn_3Te_5$), CSD-429085 ($Ag_{0.2}Cd_{0.75}In_{2.1}Te_4$), CSD-429088 ($AgIn_5Te_8$), and CSD-429087 ($Ag_{0.25}Cd_{0.5}In_{2.25}Te_4$) as well as the names of the authors and citation of the paper (fax: +49-7247-808-666; e-mail: crysdata@fiz-karlsruhe.de).

Physical Measurements and Band Gap Determination. Seebeck coefficients and electrical resistivities of cuboid-shaped samples (average dimension: 7 × 2.5 × 3 mm^3) were measured with a Linseis LSR-3 apparatus equipped with two K-type (Ni/CrNi) thermocouples (average distance: 6 mm) and Ni electrodes under a static He atmosphere. A current of 100 mA was applied to measure two data points (merged afterward) in steps of 25 °C between 50 and 400 °C, applying a bipolar measurement series (i.e., inverting the polarity of the electrodes) in high-resistance measurement mode. In this two-point setup, the absolute value of the electrical conductivity is almost unaffected by contact resistance due to the high resistivity of the samples. The measured values are affected by a typical uncertainty of 10%. The band gap was calculated using the Goldsmid−Sharp

DOI: 10.1021/acs.inorgchem.5b00433
Inorg. Chem. 2015, 54, 5745−5756

Table 1. Crystallographic Data and Details of the Structure Refinement of $AgIn_3Te_5$ = $Ag_{0.8}In_{2.4}Te_4$ at Room Temperature

	$Ag_{0.8}In_{2.4}Te_4$			
formula mass (in g mol^{-1})	1744.51			
cell parameters (in Å)	a = 6.249 29(3), c = 12.499 88(9)			
cell volume (in Å^3)	488.166(6)			
cryst syst/space group	tetragonal/$P\bar{4}2c$			
X-ray density (in g cm^{-1})	5.93			
formula units per unit cell	2			
F(000)	726			
params/thereof background	147/96			
R_p (all data sets)	0.086			
R_{wp} (all data sets)	0.114			
GooF (all data sets)	1.80			
	away from edges	Te-K edge	In-K edge	Ag-K edge
wavelength (in Å)	0.354 198(10)[a]	0.389 687(1)	0.443 758(1)	0.485 883(1)
energy (in keV)	35.00422	31.81637	27.93961	25.51731
measd reflns	515	551	551	565
absorp coeff μ (in mm^{-1})	16.5	12.3	8.4	7.2
2θ range (in deg)	3−30	3−34	3−39	3−43.5
sin ϑ_{max}/λ in Å^{-1}	0.73	0.75	0.75	0.75
$\Delta f'/\Delta f''$ of the absorbing element		−7.43/3.45	−8.13/1.86	−9.28/2.49
R_{Bragg}	0.033	0.029	0.029	0.034
R_p	0.089	0.078	0.078	0.104
R_{wp}	0.117	0.100	0.105	0.131
GooF	2.17	1.38	1.79	1.82

[a]Value determined using a Si standard sample (NIST 670c); other wavelengths refined.

Table 2. Atom Parameters of $AgIn_3Te_5$ = $Ag_{0.8}In_{2.4}Te_4$ at Room Temperature: Atom Positions and Coordinates, Occupancy Factors (Missing esd's Are Due to Constraints), and Isotropic Displacement Parameters (B_{eq} in Å^2)

atom	Wyckoff	x	y	z	occupancies	B_{eq}
Ag/In	2e	0	0	0	0.20(5)/0.73(6)	1.6(2)
Ag/In	2f	0.5	0.5	0	0.20(6)/0.71(7)	2.1(2)
Ag/In	2b	0.5	0	0.25	0.20(2)/0.24(2)	3.3(2)
Ag/In	2d	0	0.5	0.25	0.20/0.72	2.10(7)
Te	8n	0.265(2)	0.233(2)	0.13249(13)	1	2.46(2)

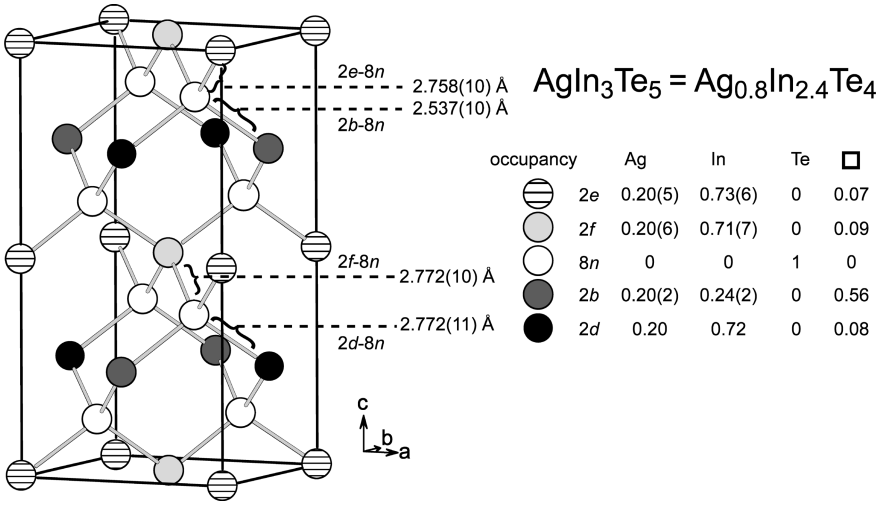

Figure 2. Occupancy factors for each position and bond lengths in the refined model of $AgIn_3Te_5$ = $Ag_{0.8}In_{2.4}Te_4$ at 293 K; missing esd's are due to parameter constraints.

method,[55] $E_g = 2eS_{max}T_{max}$, where S is the Seebeck coefficient, T the temperature, and e the elemental charge, as well as from an Arrhenius plot of the electrical conductivity in the temperature interval of intrinsic semiconduction.

RESULTS AND DISCUSSION

General Aspects. All syntheses yielded single-phase products according to their powder diffraction patterns, all of which were fitted by the Rietveld method (see below and

DOI: 10.1021/acs.inorgchem.5b00433
Inorg. Chem. 2015, 54, 5745−5756

figures in the Supporting Information). Annealing did not change the patterns significantly. In the case of joint refinements on resonant diffraction data, tentative refinements did not hint at any kind of anti-site disorder. Therefore, full occupancy of anion sites by Te was assumed, and the site occupancies of all cations on all Wyckoff sites were refined, constrained in a way that the overall composition meets the sum formula. For each Wyckoff position, an individual isotropic displacement parameter was refined.

The homogeneity of the bulk samples was further confirmed by SEM or TEM EDX measurements, respectively, for $AgIn_3Te_5$ (nominal: $Ag_{11.1}In_{33.3}Te_{55.6}$; measured: $Ag_{11.0(5)}In_{33.8(4)}Te_{55.3(3)}$; SEM, average of 15 points), $Ag_{0.2}Cd_{0.75}In_{2.1}Te_4$ (nominal: $Ag_{2.8}Cd_{10.6}In_{29.8}Te_{56.7}$; measured: $Ag_{4.4(5)}Cd_{12.8(4)}In_{28.3(9)}Te_{54.6(12)}$; TEM, average of 10 points), $AgIn_5Te_8$ (nominal: $Ag_{7.1}In_{35.7}Te_{57.1}$; measured: $Ag_{7.9(3)}In_{36.0(2)}Te_{56.2(3)}$; SEM, average of 12 points), and $Ag_{0.25}Cd_{0.5}In_{2.25}Te_4$ (nominal: $Ag_{3.6}Cd_{7.1}In_{32.1}Te_{57.1}$; measured: $Ag_{3.8(2)}Cd_{7.9(2)}In_{32.6(2)}Te_{55.8(3)}$; SEM, average of 12 points). In nonrepresentative parts of the sample with the composition $Ag_{0.2}Cd_{0.75}In_{2.1}Te_4$, however, a TEM investigation (cf. Figure S24 in the Supporting Information) revealed small amounts of a Ag-rich impurity phase (most likely Ag_9In_4), which does not significantly contribute to the diffraction pattern.

Structure of $AgIn_3Te_5 = Ag_{0.8}In_{2.4}Te_4$. The comparison of Pawley and Rietveld refinements for $AgIn_3Te_5$ (= $Ag_{0.8}In_{2.4}Te_4$, which with $Z = 2$ corresponds to the unit cell content) assuming different tetragonal and lower symmetries confirmed the space group $P\bar{4}2c$ in accordance with an earlier structure determination,[27] which also relied on Rietveld refinements and SAED patterns. In that study, In is assumed to occupy the Wyckoff sites 2*b* (s.o.f. 0.4), 2*d* (s.o.f. 1), and 2*f* (s.o.f. 1), whereas Ag is assumed to concentrate on 2*e* (s.o.f. 0.4). In the present study, anomalous dispersion effects clearly reveal cation disorder. The cation and vacancy distribution in $AgIn_3Te_5$ was refined with the constraint imposed by the sum formula (for other refinement details see the Experimental Section). Rietveld profile fits for $AgIn_3Te_5$ are shown in Figure 1, and the results of the refinements are given in Tables 1 and 2 as well as represented in Figure 2.

The structure of $AgIn_3Te_5$ formally consists of an alternating arrangement of anion and two different types of cation layers stacked along [001]. Type A cation layers contain the Wyckoff sites 2*e* and 2*f*, whereas type B layers contain the sites 2*b* and 2*d*. These layers are connected via Te atoms so that they form a diamond-like network with tetrahedral coordination of all atom sites. The element distribution on the positions 2*e*, 2*f*, and 2*d* is very similar to ∼70% In and ∼20% Ag, whereas position 2*b* contains equal amounts of In and Ag in addition to the majority of vacancies (56%). These findings are supported by bond-valence sums (BVS, calculated with the program VALIST[56] using bond-valence parameters taken from ref 57, cf. Table S6 and Figure S26). The BVS of the Te site amounts to 2.6(2) and matches the expected value of 2 (the individual valence contributions were weighted with the occupancy factors of the respective cations, and the standard deviation was estimated from those of the occupancy factors and bond lengths). The atomic displacement parameters of the cations are in the same range for positions 2*e*, 2*f*, and 2*d*, while the higher value for position 2*b* (3.3(2) Å^2) is probably due to the different occupancies and the high vacancy concentration. The vacancies on 2*b* involve a shift of the neighboring Te atoms toward this position, as evidenced by a shorter bond length to neighboring Te atoms compared to the other cation−tellurium bond lengths (cf. Figure 2). As a consequence, cation-centered tetrahedra are distorted with bond angles between 106.09° and 116.0°. $AgInTe_2$, in comparison, has no vacancies and is ordered, which results in longer Ag−Te (2.8045 Å) and shorter In−Te (2.7402 Å) bond lengths and angles closer to the ideal tetrahedral angle (108.5−111.4°).[58]

$Ag_{0.2}Cd_{0.75}In_{2.1}Te_4$: An Example from the Solid Solution Series $(CdIn_2Te_4)_x(Ag_{0.8}In_{2.4}Te_4)_{1-x}$. Compounds of the solid solution $(CdIn_2Te_4)_x(Ag_{0.8}In_{2.4}Te_4)_{1-x}$ show a Vegard-like behavior of the lattice parameters for compounds with $x > 0.5$ (cf. Figure S25 in the Supporting Information in combination with results of Rietveld refinements of $Ag_{0.4}Cd_{0.5}In_{2.2}Te_4$, i.e., $x = 0.5$, from laboratory diffraction data, cf. Figure S19 and Tables S4 and S5). A complete solid solution is not expected, as the end members exhibit nonisotypic structures with different space groups ($Ag_{0.8}In_{2.4}Te_4 = AgIn_3Te_5$: $P\bar{4}2c$; $CdIn_2Te_4$: $I\bar{4}2m$). $CdIn_2Te_4$ has recently been shown to crystallize in the $HgCu_2I_4$ structure type, a defect variant of the chalcopyrite type, with disordered cations and 25% cation vacancies.[35] A structure model for $Ag_{0.2}Cd_{0.75}In_{2.1}Te_4$ was established after tentative refinements using the Pawley and Rietveld methods, the latter with various reasonable structural models with different symmetries. In addition to a completely disordered model (sphalerite type, $F\bar{4}3m$), the structure models of the end members $CdIn_2Te_4$ and $Ag_{0.8}In_{2.4}Te_4$ were taken into account. Based on group−subgroup relationships starting from $I\bar{4}2m$, the space groups $I\bar{4}$, *I*222, *Fmm*2, *C*2, and *Cm* were tested, as well as $P\bar{4}$, *P*222, *Ccc*2, *P*2, and *Cc* starting from $P\bar{4}2c$. No significant deviation from tetragonal symmetry was evident, neither concerning the lattice parameters nor the atom positions. The Vegard-like behavior further indicates that the structure type of the end member $CdIn_2Te_4$ with the space group $I\bar{4}2m$ is retained. Thus, the model was modified in a way that all cations share all cation positions (tentative refinements indicated no vacancies on these positions). In addition, the Wyckoff site 2*b* (1/2 1/2 0), which is not occupied in $CdIn_2Te_4$, was allowed, as $Ag_{0.2}Cd_{0.75}In_{2.1}Te_4$ exhibits fewer (23.75%) cation vacancies than $CdIn_2Te_4$ (25%). This is corroborated by difference Fourier syntheses showing significant electron density. All positions except 2*b* turned out to be fully occupied. Tentative refinements indicated that the site 2*b* is most likely occupied by Ag; however, due to the low occupancy, other elements cannot be excluded but were not taken into account in the refinement. The results of the refinement are shown in Figure 3 as well as Tables 3 and 4. The structure is visualized in combination with site occupancies in Figure 4.

The structure of $Ag_{0.2}Cd_{0.75}In_{2.1}Te_4$ may formally be described as a stacking of anion and cation layers along [001]. Whereas the former belong to one Wyckoff site (8*i*), the latter alternatingly correspond to Wyckoff sites 4*d* (type B) and 2*a* and 2*b* (type A), respectively. The element distribution on 4*d* and 2*a* is similar (cf. Figure 4), while the high vacancy concentration in 2*b* corresponds to the unoccupied position in $CdIn_2Te_4$. Cd and In are uniformly distributed in both $CdIn_2Te_4$ and $Ag_{0.2}Cd_{0.75}In_{2.1}Te_4$, which results in a similar charge distribution in both compounds.[35] The bond lengths are shorter if they involve the vacancy-containing position 2*b*; that is, Te atoms are displaced toward the vacancies. The tetrahedra around cations are slightly distorted with bond angles ranging between 103.62° and 119.50°.

DOI: 10.1021/acs.inorgchem.5b00433
Inorg. Chem. 2015, 54, 5745−5756

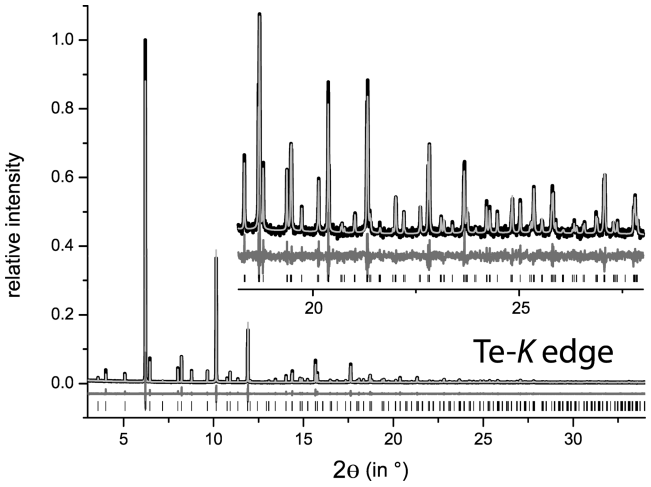

Figure 3. Results of the joint Rietveld refinement for $Ag_{0.2}Cd_{0.75}In_{2.1}Te_4$, exemplarily shown for the data set at 0.389 618(1) Å (i.e., at the Te-K edge); vertical lines indicate calculated reflection positions, experimental (black) and calculated intensities (gray) as well as difference plots (below; same intensity scale as the diffraction patterns) are shown (inset: enlargement of the high-angle region); further enlarged patterns for all five data sets used are given in the Supporting Information (Figures S5–S9).

Structure of $AgIn_5Te_8$ = $Ag_{0.5}In_{2.5}Te_4$. Previous investigations reported the space group $I\bar{4}$ or $P\bar{4}2m$ for $AgIn_5Te_8$ (=$Ag_{0.5}In_{2.5}Te_4$); however, no unequivocal evidence was given.[9,17−19] The reflection condition for body centering ($h + k + l = 2n$) was analyzed in a diffraction pattern measured at the Ag-K absorption edge (cf. Figure 5), i.e., with enhanced scattering contrast. In a simulated pattern assuming the space group $P\bar{4}2m$ (model taken from ref 19), the reflections 205, 223, 311, and 313 are clearly visible and do not overlap with reflections with $h + k + l = 2n$. As none of these reflections were observed, body-centered structure models ($I\bar{4}$, $I\bar{4}2m$), which were reported for compounds with defect chalcopyrite-type structures, were tested in tentative joint refinements with data measured at the K absorption edges. No evidence for symmetries lower than $I\bar{4}2m$ was found, and even orthorhombic or lower symmetries yielded no improvement. These findings were verified by comparing SAEDs with simulated ones (cf. Figure 6). For zone axes [$2\bar{2}1$] and [011], no reflections break the reflection condition $h + k + l = 2n$.

As the situation is comparable to that of $CdIn_2Te_4$, which exhibits the same anion/cation ratio as $AgIn_5Te_8$, a $HgCu_2I_4$-type model[35] was modified in a way that all cations share all Wyckoff sites. The refinement (cf. Figure 7) is satisfactory, and no significant residual electron density was detected in difference Fourier maps. The results of the refinement are given in Figure 8 (bold face type) as well as Tables 5 and 6.

In the $HgCu_2I_4$-type structure of $AgIn_5Te_8$ (= $Ag_{0.5}In_{2.5}Te_4$), the cation layers (see above) correspond to the Wyckoff sites 4*d* and 2*a* (plus vacancies), respectively. There is a slight preference of Ag on position 2*a* (0.193) compared to 4*d* (0.153), which is comparable to the cation distribution in $CdIn_2Te_4$.[19] The bond length is slightly shorter for 4*d*−8*i* (2.7826(9) Å) than for 2*a*−8*i* (2.7982(8) Å), which is most likely due to 4*d* bearing more In^{3+}, which has a smaller ionic radius (0.76 Å) than Ag^+ (1.14 Å).[59] The angles in the distorted cation-centered tetrahedra range between 104.0° and 119.5°.

Solid Solution Series $(CdIn_2Te_4)_x(Ag_{0.5}In_{2.5}Te_4)_{1-x}$ and the Structure of $Ag_{0.25}Cd_{0.5}In_{2.25}Te_4$. There is a complete solid solution $(CdIn_2Te_4)_x(Ag_{0.5}In_{2.5}Te_4)_{1-x}$ ($1 \geq x \geq 0$), which shows a Vegard-like behavior of the lattice parameters (cf. Figure 9). The determination of the element distribution

Table 3. Crystallographic Data and Details of the Structure Refinement of $Ag_{0.2}Cd_{0.75}In_{2.1}Te_4$ at Room Temperature

	$Ag_{0.2}Cd_{0.75}In_{2.1}Te_4$				
formula mass (in g mol^{-1})	857.07				
cell params (in Å)	a = 6.226 87(1), c = 12.474 48(3)				
cell volume (in Å^3)	483.684(2)				
cryst syst/space group	tetragonal/$I\bar{4}2m$				
X-ray density (in g cm^{-1})	5.89				
Z	2				
F(000)	712.6				
params/thereof background	207/120				
R_p (all data sets)	0.086				
R_{wp} (all data sets)	0.120				
GooF (all data sets)	2.58				
	away from edges	Te-K edge	In-K edge	Cd-K edge	Ag-K edge
wavelength (in Å)	0.354 198(10)[a]	0.389 618(1)	0.443 662(1)	0.464 100(1)	0.485 787(1)
energy (in keV)	35.00422	31.82200	27.94565	26.71499	25.52235
measd reflns	283	299	300	301	310
absorp coeff μ (in mm^{-1})	15.6	18.0	13.5	7.8	6.8
2θ range (in °)	3−30	3−34	3−39	3−41	3−43.5
sin ϑ_{max}/λ in Å^{-1}	0.73	0.75	0.75	0.75	0.76
$\Delta f'/\Delta f''$ of the absorbing element		−7.96/2.53	−9.63/2.42	−9.49/2.27	−9.16/1.89
R_{Bragg}	0.052	0.026	0.036	0.033	0.030
R_p	0.095	0.067	0.073	0.095	0.094
R_{wp}	0.142	0.089	0.105	0.127	0.120
GooF	3.85[b]	1.63	2.46	2.46	2.33

[a]Value determined using a Si standard sample (NIST 670c); other wavelengths refined. [b]Lower sample quality than at other wavelengths (coarse powder).

DOI: 10.1021/acs.inorgchem.5b00433
Inorg. Chem. 2015, 54, 5745−5756

Table 4. Atom Parameters of $Ag_{0.2}Cd_{0.75}In_{2.1}Te_4$ at 293 K: Atom Positions and Coordinates, Occupancy Factors, and Isotropic Displacement Parameters (B_{eq} in Å^2)

atom	Wyckoff	x	y	z	occupancies	B_{eq}
Ag/Cd/In	2*a*	0	0	0	0.097/0.249/0.653	1.69(4)
Ag/Cd/In	2*b*	0.5	0.5	0	0.050/0/0	1.47[a]
Ag/Cd/In	4*d*	0	0.5	0.25	0.026(7)/0.250/0.723(7)	1.26(2)
Te	8*i*	0.27620(6)	= *x*	0.11370(10)	1	1.21(2)

[a]Average value of those for positions 2*a* and 4*d*.

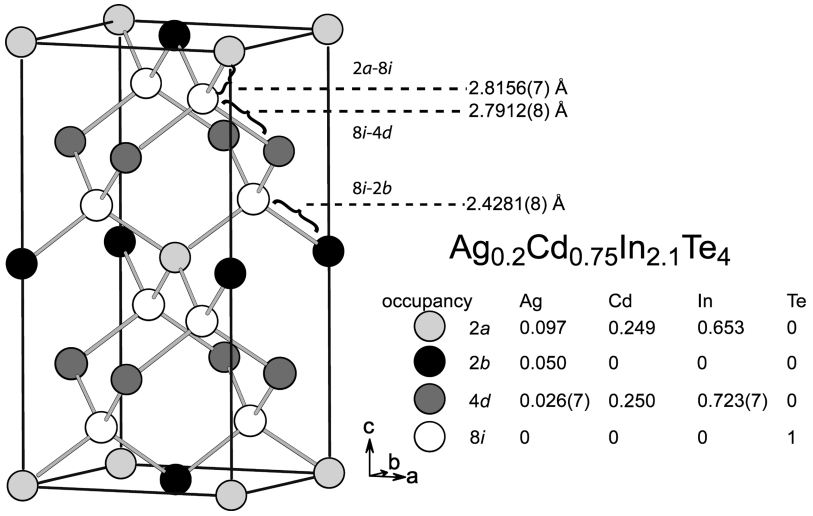

Figure 4. Occupancy factors for each position and bond lengths in the refined model of $Ag_{0.2}Cd_{0.75}In_{2.1}Te_4$ at room temperature; missing esd's are due to parameter constraints; 2*a* and 4*d* contain no significant amount of vacancies.

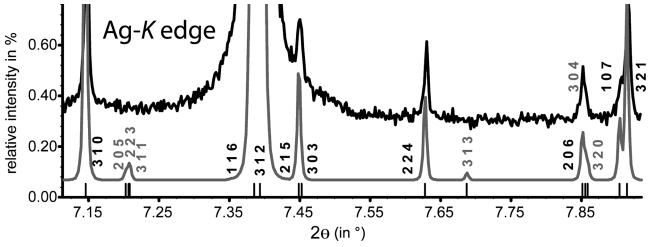

Figure 5. Comparison of an experimental powder diffraction pattern of $AgIn_5Te_8$ at the Ag-K edge (black) with a simulated one with ordered cations and vacancies in $P\bar{4}2m$[19] (below; gray): reflections with $h + k + l \neq 2n$ (indicated by gray *hkl* indices) are systematically absent due to body centering (theoretical reflection positions are indicated by vertical lines at the bottom).

based on anomalous dispersion at K-absorption edges proved successful for $x = 0.5$ assuming the $HgCu_2I_4$ type ($I\bar{4}2m$) with completely ordered vacancies formed by the end members $AgIn_5Te_8$ (= $Ag_{0.5}In_{2.5}T_4$; see above) and $CdIn_2Te_4$.[19] Again, lower symmetries yielded no improvement, and difference Fourier syntheses revealed no significant electron density on possible additional positions. The result of the refinement is shown in Figures 8 (italic type) and 10 as well as Tables 7 and 8.

The element distribution is very similar to that in $AgIn_5Te_8$, Cd replacing both Ag in In with little preference for any of the cation sites, similar to its behavior in $CdIn_2Te_4$.[19] Thus, the local charge balance remains the same as in the end members of the solid solution. Like in $AgIn_5Te_8$ (see above), the bond length 2*a*−8*i* (2.8084(3) Å) is slightly longer than 4*d*−8*i* (2.7970(3) Å). These bond lengths are closer to the

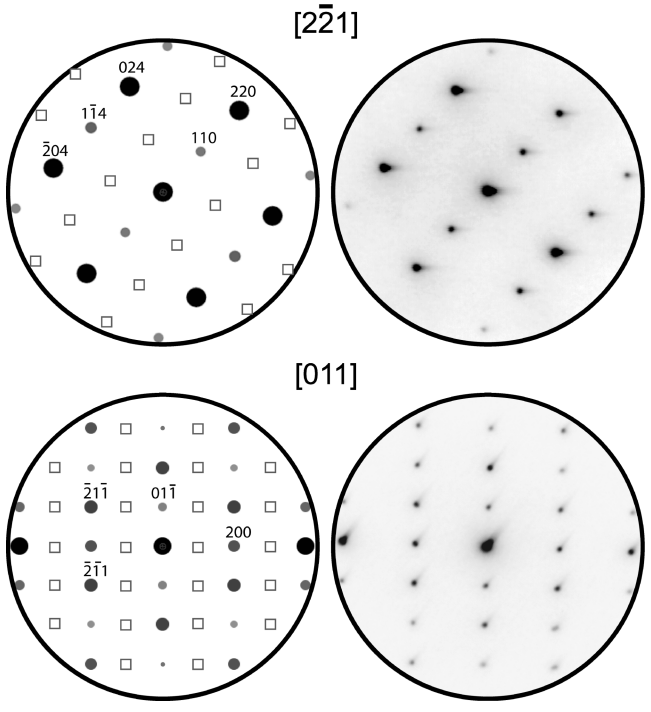

Figure 6. Comparison of experimental SAED patterns of $AgIn_5Te_8$ = $Ag_{0.5}In_{2.5}Te_4$ along the [2$\bar{2}$1] (top) and [011] (bottom) zone axes with simulated ones for a structure model with space groups $I\bar{4}2m$ (cf. Table 6) (left); additional reflection positions for $P\bar{4}2m$ are indicated by gray squares; representative reflections are indexed.

DOI: 10.1021/acs.inorgchem.5b00433
Inorg. Chem. 2015, 54, 5745−5756

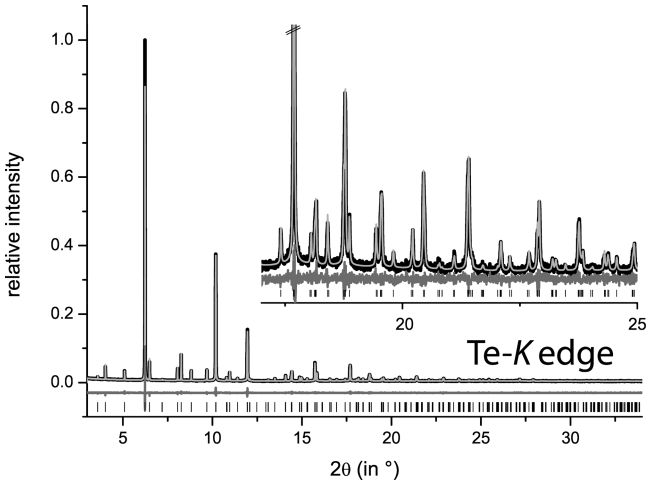

Figure 7. Results of the joint Rietveld refinement for $AgIn_5Te_8$ = $Ag_{0.5}In_{2.5}Te_4$, exemplarily shown for the data set at 0.389 712(1) Å (i.e., at the Te-K edge); vertical lines indicate calculated reflection positions; experimental (black) and calculated intensities (gray) as well as difference plots (below; same intensity scale as the diffraction patterns) are shown; enlarged patterns are shown in the Supporting Information (Figures S10–S13).

corresponding ones in $CdIn_2Te_4$ than to those in $AgIn_5Te_8$. The cation coordination tetrahedra are rather distorted with bond angles between 103.52° and 120.23°.

Physical Properties. Chalcopyrite-related materials are semiconductors, which are often strongly compensated, and therefore exhibit low electrical conductivities. The electrical band gap of compounds from the solid solution series $(CdIn_2Te_4)_x(Ag_{0.5}In_{2.5}Te_4)_{1-x}$ and $(CdIn_2Te_4)_x(Ag_{0.8}In_{2.4}Te_4)_{1-x}$ was derived from the slope of the logarithmic electrical conductivity σ versus the inverse absolute temperature (Arrhenius plot) in the intrinsic region of the semiconduction (cf. Figure 11, top) and compared with values determined from the trend of the Seebeck coefficient (cf. Figure 11 bottom) by Goldsmid and Sharp's method, an approximation that is often useful and can yield values with a reliability of about 20%.[55] All samples investigated exhibit low electrical conductivities of ca. 1 S/m. The Arrhenius plot displays the extrinsic region (~3.1–2.5 1000/K; ~50–130 °C), where there is no pronounced temperature dependence of σ, followed by the intrinsic region (~2.4–1.9 1000/K; ~150–250 °C) and, at higher temperatures, reaching saturation and therefore an almost temperature-independent σ. The Seebeck coefficients are negative and exhibit extrema at intermediate temperatures. Thus, all compounds show bipolar effects and are n-type semiconductors.

In the solid solution $(CdIn_2Te_4)_x(Ag_{0.5}In_{2.5}Te_4)_{1-x}$ (Figure 11 left), x has little influence on the Seebeck coefficients. They exhibit a peak value of ~−730 μV/mK for $Ag_{0.4}Cd_{0.2}In_{2.4}Te_4$ (x = 0.2) and $Ag_{0.1}Cd_{0.8}In_{2.1}Te_4$ (x = 0.8), while $Ag_{0.25}Cd_{0.5}In_{2.25}Te_4$ (x = 0.5) exhibits a peak value of ~−630 μV/mK and a slightly different slope. Therefore, E_g values calculated from the Seebeck coefficients[55] are rather similar for $Ag_{0.4}Cd_{0.2}In_{2.4}Te_4$ (x = 0.2) and $Ag_{0.1}Cd_{0.8}In_{2.1}Te_4$ (x = 0.8) but lower for $Ag_{0.25}Cd_{0.5}In_{2.25}Te_4$ (x = 0.5), as shown in Table 9. E_g values determined from the Arrhenius plot are lower and decrease from 0.47 eV for $Ag_{0.5}In_{2.5}Te_4$ to 0.29 for $Ag_{0.1}Cd_{0.8}In_{2.1}Te_4$ (x = 0.8), whereas a much higher value of 1.37 eV was reported for $CdIn_2Te_4$.[32] This is most likely due to the more covalent bonding character of $CdIn_2Te_4$, which results in a rather large band gap.

In the case of $(CdIn_2Te_4)_x(Ag_{0.8}In_{2.4}Te_4)_{1-x}$, E_g values determined differ strongly for the two methods (cf. Table 9). Yet, the E_g calculated from the Seebeck coefficients of $Ag_{0.2}Cd_{0.75}In_{2.1}Te_4$ is probably rather imprecise as the extremum is very flat (x = 0.75; ~−300 μV/mK). Probably, the assumptions of Goldsmid and Sharp's method are not valid for these compounds.

CONCLUSION

Both the lacking scattering contrast in chalcopyrite-related Cd/Ag/In tellurides and unsolved problems concerning their symmetry could be overcome by the analysis of X-ray powder diffraction patterns collected at K-absorption edges of Ag, Cd, In, and Te in combination with electron diffraction. In the solid solution $(CdIn_2Te_4)_x(Ag_{0.8}In_{2.4}Te_4)_{1-x}$, the different structure types of the end members lead to a miscibility gap for x < 0.5. It is a general trend that vacancies tend to order while cations remain disordered. Te atoms move toward the vacancies. In the

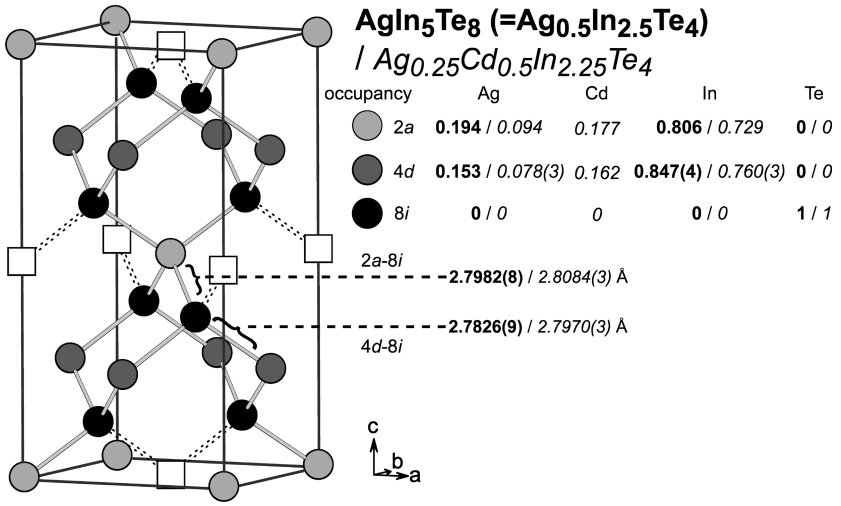

Figure 8. Occupancy factors and bond lengths in the refined model of $AgIn_5Te_8$ = $Ag_{0.5}In_{2.5}Te_4$ (bold face type) and $Ag_{0.25}Cd_{0.5}In_{2.25}Te_4$ (italic type) at room temperature; missing esd's are due to parameter constraints.

DOI: 10.1021/acs.inorgchem.5b00433
Inorg. Chem. 2015, 54, 5745–5756

Table 5. Crystallographic Data and Details of the Structure Refinement of $AgIn_5Te_8$ = $Ag_{0.5}In_{2.5}Te_4$ at Room Temperature

	$Ag_{0.5}In_{2.5}Te_4$			
formula mass (in g mol^{-1})	851.83			
cell params (in Å)	a = 6.203 68(1), c = 12.432 58(4)			
cell volume (in Å^3)	478.476(2)			
cryst syst/space group	tetragonal/$I\bar{4}2m$			
X-ray density (in g cm^{-1})	5.91			
formula units per unit cell	2			
F(000)	708			
params/thereof background	154/96			
R_p (all data sets)	0.052			
R_{wp} (all data sets)	0.072			
GooF (all data sets)	1.55			
	away from edges	Te-K edge	In-K edge	Ag-K edge
wavelength (in Å)	0.354 198(10)[a]	0.389 712(1)	0.443 719(1)	0.485 899(1)
energy (in keV)	35.004 22	31.814 32	27.942 06	25.516 47
measd reflns	276	297	298	310
absorp coeff μ (in mm^{-1})	16.5	12.1	8.0	6.9
2θ range (in deg)	3−30	3−34	3−39	3−43.5
sin ϑ_{max}/λ in Å^{-1}	0.73	0.75	0.75	0.76
$\Delta f'/\Delta f''$ of the absorbing element		−8.12/2.43	−8.45/2.43	−8.52/2.02
R_{Bragg}	0.022	0.017	0.018	0.022
R_p	0.058	0.050	0.050	0.067
R_{wp}	0.076	0.063	0.065	0.085
GooF	1.86	1.36	1.56	1.47

[a]Value determined using a Si standard sample (NIST 670c); other wavelengths refined.

Table 6. Atom Parameters of $AgIn_5Te_8$ = $Ag_{0.5}In_{2.5}Te_4$ at Room Temperature: Atom Positions and Coordinates, Occupancy Factors, and Isotropic Displacement Parameters (B_{eq} in Å^2)

atom	Wyckoff	x	y	z	occupancies	B_{eq}
Ag/In	2a	0	0	0	0.194/0.806	1.87(3)
Ag/In	4d	0	0.5	0.25	0.153/0.847(4)	1.59(2)
Te	8i	0.27546(5)	=x	0.11345(12)	1	1.41(2)

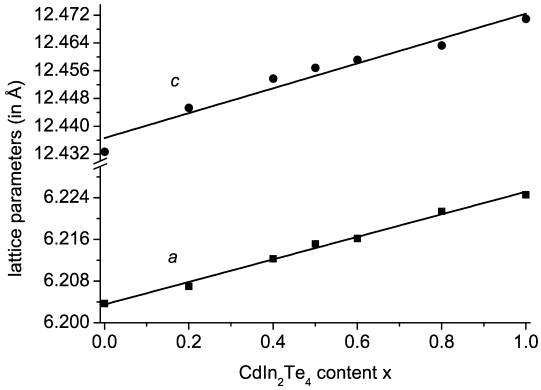

Figure 9. Vegard behavior of the lattice parameters of $(CdIn_2Te_4)_x(Ag_{0.5}In_{2.5}Te_4)_{1-x}$, namely, $AgIn_5Te_8$ = $Ag_{0.5}In_{2.5}Te_4$ (x = 0), $Ag_{0.4}Cd_{0.2}In_{2.4}Te_4$ (x = 0.2), $Ag_{0.3}Cd_{0.4}In_{2.3}Te_4$ (x = 0.4), $Ag_{0.25}Cd_{0.5}In_{2.25}Te_4$ (x = 0.5), $Ag_{0.2}Cd_{0.6}In_{2.2}Te_4$ (x = 0.6), $Ag_{0.1}Cd_{0.8}In_{2.1}Te_4$ (x = 0.8), and $CdIn_2Te_4$ (x = 1) (some lattice parameters taken from laboratory data sets; cf. Tables S2 and S3 and Figures S19−S23 in the Supporting Information).

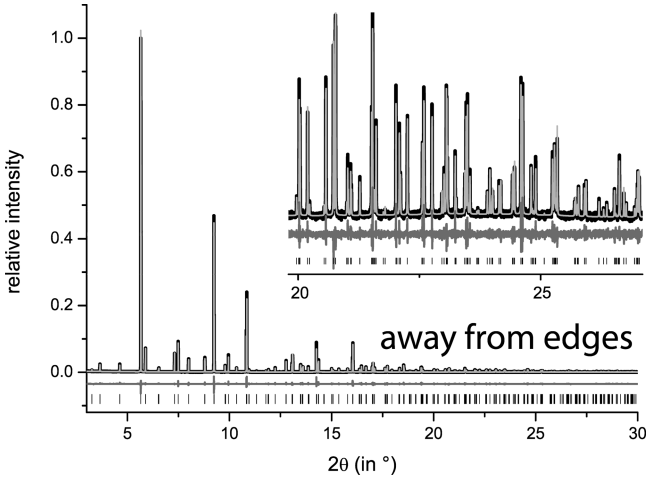

Figure 10. Results of the joint Rietveld refinement for $Ag_{0.25}Cd_{0.5}In_{2.25}Te_4$, exemplarily shown for the data set at 0.354 198(10) Å (i.e., away from the edges); vertical lines indicate calculated reflection positions; experimental (black) and calculated intensities (gray) as well as difference plots (below; same intensity scale as the diffraction patterns) are shown (enlarged patterns for all wavelengths used are depicted in the Supporting Information, Figures S14−S18).

end member $AgIn_3Te_5$ = $Ag_{0.8}In_{2.4}Te_4$, vacancies concentrate on position 2b (60%) and are mixed with equal amounts of Ag and In, while all other positions exhibit only small amounts of vacancies (∼10%) and the majority of In. This arrangement means that the anions are uniformly surrounded by cations and the vacancies are ordered on one special position where cations would exhibit unfavorably high bond-valence sums. The small amount of vacancies on the remaining positions is compensat-

DOI: 10.1021/acs.inorgchem.5b00433
Inorg. Chem. 2015, 54, 5745−5756

Table 7. Crystallographic Data and Details of the Structure Refinement of $Ag_{0.25}Cd_{0.5}In_{2.25}Te_4$ at Room Temperature

	$Ag_{0.25}Cd_{0.5}In_{2.25}Te_4$				
formula mass (in g mol^{-1})	851.92				
cell params (in Å)	a = 6.213 42(1), c = 12.456 43(1)				
cell volume (in Å^3)	480.900(3)				
cryst syst/space group	tetragonal/$I\bar{4}2m$				
X-ray density (in g cm^{-1})	5.88				
formula units (per unit cell)	2				
F(000)	708				
params/thereof background	192/120				
R_p (all data sets)	0.078				
R_{wp} (all data sets)	0.099				
GooF (all data sets)	1.40				
	away from edges	Te-K edge	In-K edge	Cd-K edge	Ag-K edge
wavelength (in Å)	0.354 198(10)[a]	0.389 746(1)	0.443 785(1)	0.464 163(1)	0.485 919(1)
energy (in keV)	35.004 22	31.811 55	27.937 91	26.711 36	25.515 42
measd reflns	279	297[b]	297[b]	299[b]	309[b]
absorp coeff μ (in mm^{-1})	16.4	11.7	8.3	6.9	6.8
2θ range (in °)	3−30	3−34	3−39	3−41	3−43.5
sin ϑ_{max}/λ in Å^{-1}	0.73	0.75	0.75	0.75	0.76
$\Delta f'/\Delta f''$ of the absorbing element		−8.17/2.62	−7.42/1.03	−9.72/2.65	−8.44/2.12
R_{Bragg}	0.033	0.068	0.039	0.044	0.042
R_p	0.076	0.065	0.073	0.093	0.095
R_{wp}	0.099	0.082	0.092	0.114	0.117
GooF	1.61	1.26	1.52	1.33	1.30

[a]Value determined using a Si standard sample (NIST 670c); other wavelengths refined. [b]The 112 reflection (which is the strongest) is probably affected by dead-time problems of the detector. An approach to implement an extinction correction (similar to the one in SHELXL[60]) yielded no significant improvement. Therefore, the reflection was excluded from the refinement for the data sets measured at the K-absorption edges.

Table 8. Atom Parameters of $Ag_{0.25}Cd_{0.5}In_{2.25}Te_4$ at Room Temperature: Atom Positions and Coordinates, Occupancy Factors, and Isotropic Displacement Parameters (B_{eq} in Å^2)

atom	Wyckoff	x	y	z	occupancies	B_{eq}
Ag/Cd/In	2a	0	0	0	0.094/0.177/0.729	1.560(14)
Ag/Cd/In	4d	0	0.5	0.25	0.078(3)/0.162/0.760(3)	1.318(9)
Te	8i	0.27711(3)	=x	0.11233(4)	1	1.143(10)

ing the anions that are facing additional Ag atoms on one side. The space group $P\bar{4}2c$ was correctly determined in previous studies;[27] however, the assumed ordered element distribution is not confirmed by resonant X-ray diffraction. Long-range order was not observed, but it appears likely that there is a certain degree of short-range order within domains sized smaller than the X-ray's length of coherence. $Ag_{0.2}Cd_{0.75}In_{2.1}Te_4$ (x = 0.75) exhibits a comparable tendency toward vacancy ordering in the $HgCu_2I_4$ structure type of the end member $CdIn_2Te_4$.[35] The cations are uniformly distributed, and the vacancy positions of $CdIn_2Te_4$ are partially filled in solid solutions with higher cation/anion ratio. $Ag_{0.5}In_{2.5}Te_4$ and $Ag_{0.25}Cd_{0.5}In_{2.25}Te_4$ (x = 0.5), which are members of the solid solution series $(CdIn_2Te_4)_x(Ag_{0.5}In_{2.5}Te_4)_{1-x}$, also exhibit $HgCu_2I_4$-type structures with completely ordered vacancies and disordered cations. As the cation/anion ratio is constant, no vacancies are filled when x is changed.

The differences between the band gaps E_g calculated from the electrical conductivites and the Seebeck coefficients, respectively, are most likely due to the fact than the approximations presumed by Goldsmid and Sharp[55] are not valid in this case. This method assumes that the carriers' effective mass is isotropic and that they uniformly populate the band extrema (nondegenerate approximation). The Seebeck coefficient is considered to be a function of the Fermi level. Classical statistics yield two solutions for n- and p-type conduction, respectively. The majority to minority weighted mobility ratio depends on the ratio of their two effective masses. If it differs significantly from 1 or if S significantly exceeds ∼150 μV/K, the approximation may become unrealistic.[61] Values for E_g determined from the temperature dependence of the electrical conductivity indicate that the effect of the doping level is rather pronounced. The band gaps are smaller than those of other chalcopyrite-related compounds such as $AgGaTe_2$ (E_g = 1.15 eV) or $CuInTe_2$ (E_g = 0.98 eV).[7] Although the compounds investigated in this study exhibit a high S of up to −730 μV/K, comparable to other promising compounds such as $Ag_{10}Te_4Br_3$[62] or $AgBiSe_2$,[63] relevant thermoelectric properties require further optimization as the electrical conductivity is still very low, probably due to the compensation of charge carriers and holes or a very low carrier mobility. Yet, chalcopyrite-related compounds with such rather low conductivities may be interesting materials for solar cell materials, as suggested for $(CdIn_2Te_4)_x(Ag_2In_2Te_4)_{1-x}$ with $x \leq$ 0.53, where optical band gaps between 0.95 and 1.13 eV were reported.[31] The knowledge of the element distribution in such compounds is important for theoretical calculations, which might be useful to predict stable configurations as well as explain the trends of physical properties. The present study

DOI: 10.1021/acs.inorgchem.5b00433
Inorg. Chem. 2015, 54, 5745−5756

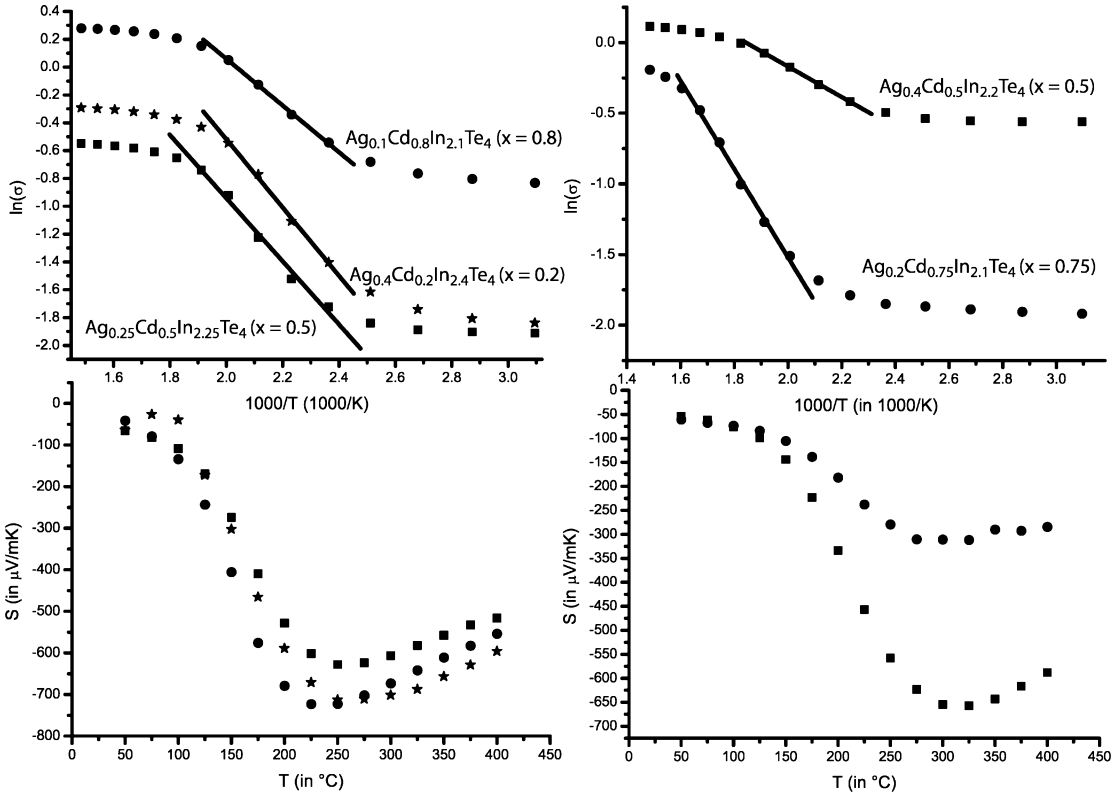

Figure 11. Plots of the logarithmic electrical conductivity versus the inverse temperature (top) and temperature-dependent Seebeck coefficients (bottom) for members of the solid solutions $(CdIn_2Te_4)_x(Ag_{0.5}In_{2.5}Te_4)_{1-x}$ (left, x = 0.2 asterisk, 0.5 square, 0.8 circle) and $(CdIn_2Te_4)_x(Ag_{0.8}In_{2.4}Te_4)_{1-x}$ (right, x = 0.5 square, 0.75 circle).

Table 9. Electrical Band Gaps of $CdIn_2Te_4$, $(CdIn_2Te_4)_x(Ag_{0.5}In_{2.5}Te_4)_{1-x}$ (x = 0.2, 0.5, 0.8, 1), and $(CdIn_2Te_4)_x(Ag_{0.8}In_{2.4}Te_4)_{1-x}$ (x = 0, 0.5, 0.75) Determined from the Electrical Conductivity and from Seebeck Coefficients[55]

compound	band gap (Seebeck[a]) (in eV)	band gap (conductivity) (in eV)
$CdIn_2Te_4$[32]		1.37
	$(CdIn_2Te_4)_x(Ag_{0.5}In_{2.5}Te_4)_{1-x}$	
$AgIn_5Te_8$ (= $Ag_{0.5}In_{2.5}Te_4$)[21]	0.27	0.47
$Ag_{0.4}Cd_{0.2}In_{2.4}Te_4$ (x = 0.2)	0.75	0.42
$Ag_{0.25}Cd_{0.5}In_{2.25}Te_4$ (x = 0.5)	0.66	0.39
$Ag_{0.1}Cd_{0.8}In_{2.1}Te_4$ (x = 0.8)	0.72	0.29
	$(CdIn_2Te_4)_x(Ag_{0.8}In_{2.4}Te_4)_{1-x}$	
$AgIn_3Te_5$ (= $Ag_{0.8}In_{2.4}Te_4$)[22]	0.65	0.68
$Ag_{0.4}Cd_{0.5}In_{2.2}Te_4$ (x = 0.5)	0.78	0.19
$Ag_{0.2}Cd_{0.75}In_{2.1}Te_4$ (x = 0.75)	0.37	0.54

[a]Some Seebeck coefficients and conductivities were taken from the literature as referenced.

shows that calculations for simplified ordered models may not well describe the actual situation that is dominated by disorder.

■ ASSOCIATED CONTENT

Supporting Information

Detailed synthesis conditions, enlarged Rietveld plots for all data sets, additional tables for Rietveld refinements performed for lattice parameter determination, a Vegard plot, details on bond-valence calculations, and a TEM investigation of $Ag_{0.2}Cd_{0.75}In_{2.1}Te_4$. This material is available free of charge via the Internet at http://pubs.acs.org.

■ AUTHOR INFORMATION

Corresponding Author

*E-mail: oliver.oeckler@gmx.de. Tel: +49-(0)341-9736251. Fax: +49-(0)341-9736299.

Notes

The authors declare no competing financial interest.

■ ACKNOWLEDGMENTS

The authors thank Dr. Thorsten Schröder for help during the synchrotron measurements. The ESRF is gratefully acknowledged for the support of this work (project HS-4826). Part of this investigation was funded by the Deutsche Forschungsgemeinschaft (grant OE530/1-2).

■ REFERENCES

(1) Green, M. A.; Emery, K.; Hishikawa, Y.; Warta, W. *Prog. Photovolt.: Res. Appl.* **2010**, *18*, 346−352.

(2) Reinhard, P.; Buecheler, A. S.; Tiwari, A. N. *Sol. Energy Mater. Sol. Cells* **2013**, *119*, 287−290.

(3) Fan, F.-J.; Wu, L.; Yu, S.-H. *Energy Environ. Sci.* **2014**, *7*, 190−208.

DOI: 10.1021/acs.inorgchem.5b00433
Inorg. Chem. 2015, 54, 5745−5756

(4) Jager-Waldau, A. *Sol. Energy Mater. Sol. Cells* **2011**, *95*, 1509−1517.
(5) Mitzi, D. B.; Gunawan, O.; Todorov, T. K.; Wang, K.; Guha, S. *Energy Mater. Sol. Cells* **2011**, *95*, 1421−1436.
(6) Yusufu, A.; Kurosaki, K.; Kosuga, A.; Sugahara, T.; Ohishi, Y.; Muta, H.; Yamanaka, S. *Appl. Phys. Lett.* **2011**, *99*, 061902.
(7) Parker, D.; Singh, D. J. *Phys. Rev. B* **2012**, *85*, 125209.
(8) Wu, W.; Wu, K.; Ma, Z.; Sa, R. *Chem. Phys. Lett.* **2012**, *537*, 62−64.
(9) Bahari, Z. J.; Rivet, B.; Dugué, J. *C. R. Acad. Sci. Ser. II C* **1998**, *1*, 411−415.
(10) Bahari, Z. J.; Rivet, B.; Legendre, B.; Dugué, J. *J. Alloys Compd.* **1999**, *282*, 164−174.
(11) Chiang, P. W.; O'Kane, D. F.; Mason, D. R. *J. Electrochem. Soc.* **1967**, *114*, 759−760.
(12) O'Kane, D. F.; Mason, D. R. *J. Electrochem. Soc.* **1964**, *111*, 546−549.
(13) Frueh, A. J., Jr. *Z. Kristallogr.* **1959**, *112*, 44−52.
(14) Schneider, J.; Schulz, H. *Z. Kristallogr.* **1993**, *203*, 1−15.
(15) Zaslavskii, A. I.; Sergeeva, V. M. *Sov. Phys. Solid State* **1961**, *2*, 2556−2561.
(16) Desai, R. R.; Lakshminarayana, D.; Patel, P. B.; Patel, P. K.; Panchal, C. J. *Mater. Chem. Phys.* **2005**, *94*, 308−314.
(17) Robins, M.; Miksovsky, M. A. *Mater. Res. Bull.* **1971**, *6*, 359−364.
(18) Palatnik, L. S.; Rogacheva, E. I. *Inorg. Mater.* **1966**, *2*, 412−417.
(19) Mora, A. J.; Delgado, G. E.; Pineda, C.; Tinoco, T. *Phys. Status Solidi A* **2004**, *201*, 1477−1483.
(20) Benoit, P.; Charpin, P.; Djéga-Mariadassou, C. *Mater. Res. Bull.* **1983**, *18*, 1047−1057.
(21) Pei, Y.-L.; Zhang, C.; Li, J.; Sui, J. *J. Alloys Compd.* **2013**, *566*, 50−53.
(22) Tseng, B. H.; Wert, C. A. *J. Appl. Phys.* **1989**, *65*, 2254−2257.
(23) Hamada, T.; Yamana, A.; Nakamura, Y.; Nittono, O.; Walda, T. *Jpn. J. Appl. Phys.* **1997**, *36*, L1494−L1497.
(24) Diaz, R.; Bisson, L.; Agullo-Rueda, F.; Abd Lefdil, M.; Rueda, R. *Appl. Phys. A: Mater. Sci. Process.* **2005**, *81*, 433−438.
(25) Merino, J. M.; Mahanty, S.; Leon, M.; Diaz, R.; Rueda, F.; Martin de Vidales, J. L. *Thin Solid Films* **2000**, *361*−*362*, 70−73.
(26) Tham, A. T.; Su, D. S.; Neumann, W.; Schubert-Bischoff, P.; Beliharz, C.; Benz, K. W. *Cryst. Res. Technol.* **2000**, *35*, 823−830.
(27) Rangasami, C.; Malar, P.; Osipowicz, T.; Jain, M. K.; Kasiviswanathan, S. *Powder Diffr.* **2011**, *26*, 248−255.
(28) Díaz, M.; de Chalbaud, L. M.; Sagredo, V.; Tinoco, T.; Pineda, C. *Phys. Status Solidi B* **2000**, *220*, 281−284.
(29) Aikebaier, Y.; Kurosaki, K.; Sugahara, T.; Ohishi, Y.; Muta, H.; Yamanaka, S. *Mater. Sci. Eng., B* **2012**, *177*, 999−1002.
(30) Patel, S. M.; Patel, B. H. *Thin Solid Films* **1989**, *173*, 169−173.
(31) Cadenas, R.; Quintero, M.; Woolley, J. C. *Phys. Status Solidi A* **1994**, *144*, 311−316.
(32) O'Kane, D. F.; Mason, D. R. *J. Electrochem. Soc.* **1963**, *110*, 1132−1135.
(33) Hahn, H.; Frank, G.; Klingler, W.; Störger, A. D.; Störger, G. *Z. Anorg. Allg. Chem.* **1955**, *279*, 241−270.
(34) Launay, J.-C.; Lambert, J.-F.; Darriet, B.; Gravereau, P. *J. Mater. Chem.* **1995**, *5*, 165−169.
(35) Welzmiller, S.; Hennersdorf, F.; Fitch, A.; Oeckler, O. *Z. Anorg. Allg. Chem.* **2014**, *640*, 3135−3142.
(36) Welzmiller, S.; Urban, P.; Fahrnbauer, F.; Erra, L.; Oeckler, O. *J. Appl. Crystallogr.* **2013**, *46*, 769−778.
(37) Welzmiller, S.; Rosenthal, T.; Ganter, P.; Neudert, L.; Fahrnbauer, F.; Urban, P.; Stiewe, C.; de Boor, J.; Oeckler, O. *Dalton Trans.* **2014**, *43*, 10529−10540.
(38) Schneider, M. N.; Fahrnbauer, F.; Rosenthal, T.; Döblinger, M.; Stiewe, C.; Oeckler, O. *Chem.—Eur. J.* **2012**, *18*, 1209−1218.
(39) Urban, P.; Schneider, M. N.; Erra, L.; Welzmiller, S.; Fahrnbauer, F.; Oeckler, O. *CrystEngComm* **2013**, *15*, 4823−4829.
(40) Fahrnbauer, F.; Urban, P.; Welzmiller, S.; Schröder, T.; Rosenthal, T.; Oeckler, O. *J. Solid State Chem.* **2013**, *208*, 20−26.
(41) Oeckler, O.; Schneider, M. N.; Fahrnbauer, F.; Vaughan, G. *Solid State Sci.* **2011**, *13*, 1157−1161.
(42) Lafond, A.; Choubrac, L.; Gauillot-Deudon, C.; Fertey, P.; Evain, M.; Jobic, S. *Acta Crystallogr. Sect. B* **2014**, *70*, 390−394.
(43) Christensen, M.; Lock, N.; Overgaard, J.; Iversen, B. B. *J. Am. Chem. Soc.* **2006**, *128*, 15657−15665.
(44) Miyagawa, H.; Koshiba, S.; Takao, K.; Fujii, K.; Mizumaki, M.; Sakata, O.; Kimura, S.; Ueji, R.; Sumida, N. *Jpn. J. Appl. Phys.* **2006**, *45*, 3548−3551.
(45) Zhang, Y.; Wilkinson, A. P.; Nolas, G. S.; Lee, P. L.; Hodges, J. P. *J. Appl. Crystallogr.* **2003**, *36*, 1182−1189.
(46) Zhang, Y.; Wilkinson, A. P.; Lee, P. L.; Shastri, S. D.; Shu, D.; Chung, D.-Y.; Kanatzidis, M. G. *J. Appl. Crystallogr.* **2005**, *38*, 433−441.
(47) Stadelmann, P. *JEMS*, version 3.3525U2008; CIME-EPFL: Switzerland, 1999−2008.
(48) Hodeau, J.-L.; Bordet, P.; Anne, M.; Prat, A.; Fitch, A. N.; Dooryhee, E.; Vaughan, G.; Freund, A. *Proc. SPIE* **1998**, *3448*, 353.
(49) Wright, J. P.; Vaughan, G. B. M.; Fitch, A. N. *IUCr Comput. Commission Newslett.* **2003**, *1*, 92.
(50) de L. Kronig, R. *J. Opt. Soc. Am.* **1926**, *12*, 547−556.
(51) Evans, G.; Pettifer, R. F. *J. Appl. Crystallogr.* **2001**, *34*, 82−86.
(52) Henke, B. L.; Gullikson, E. M.; Davis, J. C. *Atom. Data Nucl. Data* **1993**, *54*, 181−342.
(53) Coelho, A. *TOPAS Academic*, V. 4.1; Coelho Software: Brisbane, 2007.
(54) Stephens, P. W. *J. Appl. Crystallogr.* **1999**, *32*, 281−289.
(55) Goldsmid, H. J.; Sharp, J. W. *J. Electron. Mater.* **1999**, *28*, 869−872.
(56) Wills, A. S. *VaList*; Program available from www.ccp14.ac.uk.
(57) Brese, N. E.; O'Keeffe, M. *Acta Crystallogr. Sect. B* **1991**, *47*, 192−197.
(58) Moustafa, A. M.; El-Sayad, E. A.; Sakr, G. B. *Cryst. Res. Technol.* **2004**, *39*, 266−273.
(59) Shannon, R. D. *Acta Crystallogr., Sect. A* **1976**, *32*, 751−767.
(60) Sheldrick, G. M. *Acta Crystallogr., Sect. A* **2008**, *64*, 112−122.
(61) Gibbs, Z. M.; Kim, H.-S.; Wang, H.; Snyder, G. J. *Appl. Phys. Lett.* **2015**, *106*, 022112.
(62) Nilges, T.; Lange, S.; Bawohl, M.; Deckwart, J. M.; Janssen, M.; Wiemhöfer, H.-D.; Decourt, R.; Chevalier, B.; Vannahme, J.; Eckert, H.; Weihrich, R. *Nat. Mater.* **2009**, *8*, 101−108.
(63) Xiao, C.; Qin, X.; Zhang, J.; An, R.; Xu, J.; Li, K.; Cao, B.; Yang, J.; Ye, B.; Xie, Y. *J. Am. Chem. Soc.* **2012**, *134*, 18460−18466.

DOI: 10.1021/acs.inorgchem.5b00433
Inorg. Chem. 2015, 54, 5745−5756